Journal of Environment Pollution and Human Health, 2022, Vol. 10, No. 2, 58-70
Available online at http://pubs.sciepub.com/jephh/10/2/4
Published by Science and Education Publishing
DOI:10.12691/jephh-10-2-4

Dynamic Adsorption on Fixed-Bed Column of Manganese Oxoanions (MnO_4^-) in Aqueous Media on Activated Carbon Prepared from Palm Nut Shells

Charly Mve Mfoumou[1,*], Pradel Tonda-Mikiela[1], Francis Ngoye[1], Mbouiti Berthy Lionel[1,2], Bouassa Mougnala Spenseur[1,2], Alexander Sachse[3], Samuel Mignard[3], Guy Raymond Feuya Tchouya[1,*]

[1]Laboratoire de Chimie des Milieux et des Matériaux Inorganiques (LC2MI), URCHI / Université des Sciences et Techniques de Masuku (USTM), BP : 943 Franceville-Gabon.
[2]Département de Chimie, Faculté des Sciences / Université des Sciences et Techniques de Masuku (USTM), BP : 943 Franceville-Gabon
[3]Institut de Chimie des Milieux et Matériaux de Poitiers (IC2MP), UMR 7285 CNRS/Université de Poitiers, 4 Rue Michel Brunet, 86022 Poitiers Cedex, France
*Corresponding author: charly.mvemfoumou@univ-masuku.org; gfeuya@yahoo.fr

Received October 17, 2022; Revised November 22, 2022; Accepted December 04, 2022

Abstract The study of the influence of operating parameters of dynamic adsorption on fixed-bed column of manganese oxoanions (MnO_4^-) in aqueous media on granular activated carbon (GAC), prepared from the shells palm nuts of Gabon, was carried out. The operating parameters studied were the particle size, the concentration of the initial solution (C_0) of MnO_4^-, the flow rate (D) and the pH of the media. The results obtained on the study of the influence of operating parameters show that the best adsorption capacities at saturation (Q_{sat}) of MnO_4^- ion on the CAG were obtained with particle size between $0.04 < x < 0.1$ (5.90 $mg.g^{-1}$); with flow rate of 3 $mL.min^{-1}$ (8.36 $mg.g^{-1}$) and when the pH of the initial solution was equal to 3.5 (27.01 $mg.g^{-1}$). Also, these results showed that the bed of prepared GAC appeared more effective when C_0 was low (10 $mg.L^{-1}$). The kinetic models of the different studies carried out show that the pseudo-first-order kinetic model best describes the adsorption of MnO_4^- ions on the GAC. The results of the intraparticle diffusion model indicate that the adsorption of MnO_4^- follows a multi-step process and that the intraparticle diffusion is not the limiting step. In addition, the surface adsorption plays a predominant role in the adsorption mechanism of MnO_4^- ions on activated carbon studied in fixed-bed column dynamics.

Keywords: *Manganese Oxoanion (MnO_4^-), activated carbon, dynamic adsorption, breakthrough curve, kinetic models*

Cite This Article: Charly Mve Mfoumou, Pradel Tonda-Mikiela, Francis Ngoye, Mbouiti Berthy Lionel, Bouassa Mougnala Spenseur, Alexander Sachse, Samuel Mignard, and Guy Raymond Feuya Tchouya, "Dynamic Adsorption on Fixed-Bed Column of Manganese Oxoanions (MnO_4^-) in Aqueous Media on Activated Carbon Prepared from Palm Nut Shells." *Journal of Environment Pollution and Human Health*, vol. 10, no. 2 (2022): 58-70. doi: 10.12691/jephh-10-2-4.

1. Introduction

Water is a natural resource essential to the life of all living beings. Unfortunately, this vital resource is often exposed to natural and/or anthropogenic pollution. Water pollution is defined as the change in the physical, chemical and biological parameters of water quality [1]. The development of mining sectors in Africa resulted in continuous pollution of this resource due to the presence of heavy metals (Cr, Mn, Co, Fe ...) in the groundwater and rivers, used in the production of drinking water. In Gabon, for example, an intensification of manganese (Mn) production in the cities of Moanda and Franceville in recent years has been observed [2]. In 2019, Gabon achieved an annual production of 6.1 million tons compared to 5.2 million tons in 2018, resulting in 17% increase in manganese production [3,4]. This strong mining activity resulted in increasing manganese concentrations in the soils and surrounding aqueous media [2]. This represents a major risk for the wellbeing of the population and the environment.

Manganese (Mn) is among inorganic pollutants sensitive to redox reactions and can form toxic MnO_4^- like oxoanions in aqueous media [5]. These species can also be formed in the disinfection process of drinking water and the removal of organic substances from wastewater by oxidation processes [6]. Although these oxidation processes are considered as promising technologies for removing organic micropollutants, they could also lead in the oxidation of inorganic ions such as chromium (Cr) and

manganese, which form unwanted oxoanions [6]. For example, manganese oxoanions, used as oxidant for liquid purification, can irritate the skin and eyes, and destroy the liver and kidneys if splashed or ingested orally [7]. Considering the harmful properties of these metal oxoanions, their elimination from industrial wastewater becomes a major threat for environmental protection and public health [8]. Thus, the World Health Organization (WHO) recommends a limit level of 0.5 $mg.L^{-1}$ of MnO_4^- ions in wastewater [9].

However, physicochemical techniques exist in the industrial sector to remove manganese oxoanions or metallic ions from industrial effluents [10,11]. These include chemical precipitation [11,13,14], chemical coagulation and flocculation [13,14,15], ion exchange [13,16,17], membrane filtration [18], electrochemical treatment [11] and adsorption processes [14,18,19,20]. Among all these techniques, adsorption processes using porous solids as adsorbents offer a simple design and operation, low and relatively inexpensive initial cost, wide adsorbents selection, and relatively inexpensive available adsorbents. This assures very accurate and efficient removal of metallic ions in wastewater [10,11].

Many studies using adsorption techniques in static (batch) for the trapping or removal of MnO_4^- ions using adsorbent materials prepared from corn cobs and animal bones [21], leaves's powders of *Azadirachta indica* [22], *Foeniculum vulgare* [23] and copper sulphide nanoparticles (CuS) [24] were reported in the literature. Activated carbons, prepared from household waste, such as coconut shells [25], are among the most widely used solid adsorbents in this type of study.

This work deals with the study of the operating parameters for optimal elimination in aqueous media of manganese oxoanions (MnO_4^-) on activated carbon, prepared from palm nuts shells collected in the city of Franceville in Gabon, in dynamic adsorption on fixed-bed column. Kinetic models of dynamic adsorption of MnO_4^- on prepared activated carbon were also carried out. The valorization of household waste, such as palm nuts shells, in the preparation of activated carbons for the elimination of mineral pollutants in aqueous media, is a second objective in this work.

2. Experimental

2.1. Source of Manganese Oxoanions (MnO_4^-)

The MnO_4^- solution used in this study was obtained from the extrapure crystallized potassium permanganate ($KMnO_4$) from Scharlab SL. 1000 $mg.L^{-1}$ of MnO_4^- solution were prepared by dissolving in distilled water 1 g of crystallized $KMnO_4$ in a flask of 1 L. The solution was stirred during 15 minutes. Then by dissolution, solutions with concentrations 10; 25 and 50 $mg.L^{-1}$ were prepared.

2.2. Adsorbent Preparation

For the preparation of activated carbon (AC), we used palm nut shells collected in the city of Franceville in the Haut Ogooué region of Gabon. The activated carbon was prepared using a chemical activation process [26]. The palm nut shells were scraped and washed several times with water, then dried in the open air during 7 days. The shells were then crushed to small particles, washed with distilled water and dried in an oven for 24 hours (h) at 383 K. These solids were then placed in a borosilicate glass crucible for preservation.

The dried palm nut shells were heat treated at 573 K for 2 h in a NABERTHEN oven before impregnation. After cooling, 50 g of the pretreated solid were impregnated with a solution of $ZnCl_2$ to 1 M (1:1 ratio) during 72 h. The impregnated solid was then dried in an oven for 24 h at 383 K. After drying, the impregnates were activated at 873 K for 1 h and 30 minutes (min) with a rise in temperature of 5 $K.min^{-1}$. The activated carbon obtained was cooled, rinsed with 0.1 M HCl, and then washed with distilled water until the pH of the residual water being equal to 6.5.

Finally, the activated carbon was dried in the oven for 48 h at 383 K and sieved to have granular activated carbons (GAC) with particle sizes $0.04 < x < 0.1$ mm; $0.1 < x < 0.25$ mm and $0.25 < x < 0.5$ mm (sieves used: TAMISAR (Norm: AFNOR_NF-X11-501).

2.3. Caracterizations

Measurements of surface area and pore volume were carried out using a Micromeritics TRISTAR 3000 instrument following T. Belin method [27]. About 100 mg of the activated carbons sample was pretreated during 1 h at 363 K, and 10 h at 623 K successively. The adsorption/desorption isotherm of nitrogen was carried out at 77 K. The specific surface areas of samples were evaluated by means of the Brunauer, Emmett and Teller (BET) theory [28]. Microporous and mesoporous volumes were determined by t-plot method of De Boer and Dubinin-Radushkevich equations respectively [29,30,31].

Quantification of surface function groups of adsorbent was performed using the Boehm method [32]. 0.2 g of solid were placed in 4 erlenmeyers of 250 mL each containing 25 mL of solutions of $NaHCO_3$, Na_2CO_3, NaOH and HCl at 0.1 N respectively. Then, the mixtures were stirred at 200 rpm during 24 h at room temperature and filtered on Büchner. Then, 10 mL of each filtrate was titrated using 0.1 N HCl (for basidic solutions) and 0.1 N NaOH (for acidic solution) in the presence of phenolphthalein and methyl orange as indicators.

The number of equivalents ($m_{eq}.g^{-1}$) or concentrations ($mmol.g^{-1}$) of acid or basic functions were determined using the following equation [33,34]:

$$n\left(mmol.g^{-1}\right) = \frac{C\ x\left(V_{eq.B} - V_{eq.E}\right) x1000}{m_{CA}}$$

Where, C is the concentration of NaOH or HCl ($mol.L^{-1}$); $V_{eq.B}$ and $V_{eq,E}$ are the equivalent volumes of the blank and sample (L) respectively; m_{CA} is the mass of activated carbon (g) and 1000 is the conversion factor in mmol.

The pH at the point of zero charge (pH_{PZC}) of activated carbon was obtained based on the method described by Amola L. A. et al. [26]. 20 mL of 0.1 M solution of KCl was introduced into 5 erlenmeyers of 50 mL. The pH of the solutions in each erlenmeyer was adjusted between 2 and 10 by adding 0.1 M HCl or NaOH solution. The pH of

these solutions were identified as the initial pH (pH_i). Then, 0.04 g of activated carbon was contacted with solutions at different pH (2; 4; 6; 8 and 10) and stirred (200 rpm) during an average time of 24 h at room temperature. Then, final pH (pH_f) of the solutions were measured. The pH_{PZC} is given by the point of intersection between the experimental curve and the theoretical curve of pHf = f(pHi).

2.4. Fixed-bed Dynamic Adsorption of MnO_4^-

Dynamic adsorption experiments on fixed-bed column of MnO_4^- were carried out at room temperature (298 K) in a pyrex brand glass column with a length of 50 cm and diameter 2.4 cm. The adsorption column consisted of a bed of granular activated carbon (GAC) of height H, sandwiched between two layers of cotton (Figure 1).

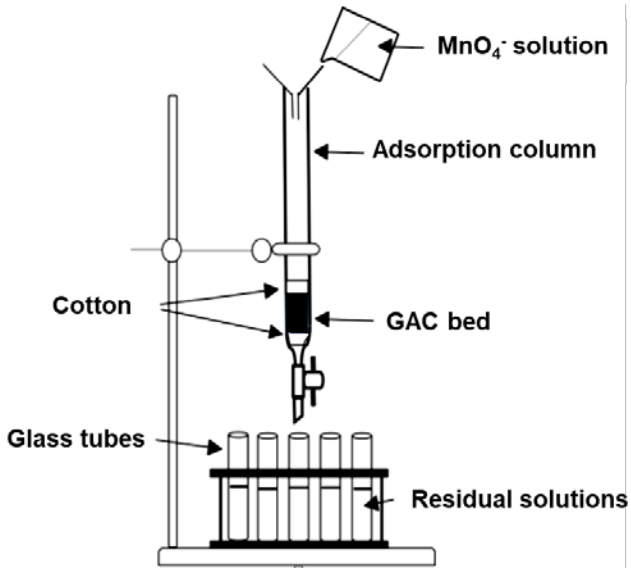

Figure 1. Scheme of the experimental set-up of the adsorption process

MnO_4^- solutions with concentration C_0 were introduced into the column, and allowed to flow by gravity through the bed of GAC with defined flow rates (D). At the outlet of the column, residual solutions of MnO_4^- with concentrations C were collected at regular time intervals (2-10 min). The residual concentrations of MnO_4^- at column output C were determined using a UV-visible molecular absorption spectrophotometer, using a calibration curve previously established at 546 nm wavelength.

Experiments on the effect of flow were carried out with flow rates of 3; 6 and 9 $mL.min^{-1}$. For the effect of particle size, experiments were conducted with activated carbon grains with particle sizes $0.04<x<0.1$ mm; $0.1<x<0.25$ mm and $0.25 < x < 0.5$ mm. Experiments on the effect of the pH of media and on the initial concentration C_0 were carried out with pH solutions of 3.5; 4.5 and 6.5 and C_0 of 10; 25 and 50 $mg.L^{-1}$ respectively.

Breakthrough curves of the dynamic adsorption of MnO_4^- ions on prepared activated carbon were plotted. These Breakthrough curves show the evolution of the ratio of concentrations at the outlet (C) and at the inlet (C_0) of the column in function of time. They give information on the efficiency of the bed to trap MnO_4^- ions, and on the adsorption mechanism of MnO_4^- on GAC.

The experiments were stopped when the beds were saturated, i.e. when the residual concentrations (C) were equal to the concentrations at the inlet of the column (C_0) ($C/C_0 = 1$). We then obtain an area (A) in minutes by integration according to the trapeze method [35]:

$$A(\min) = \sum_n \frac{\left(1-\frac{C_{t_n}}{C_0}\right)+\left(1-\frac{C_{t_{n+1}}}{C_0}\right)}{2} x\left(t_{n+1}-t_n\right)$$

Where C_0 and C are the inlet and outlet concentrations ($mg.L^{-1}$) at times t_n and t_{n+1} respectively.

The expression of the contact time (t_c) of the flow rate of MnO_4^- solution and the activated carbon bed is:

$$t_c\,(s) = \frac{H.\pi.\left(d/2\right)^2}{D} x60$$

Where H is the height of the bed (m), d is the diameter of the column (m) and D is the flow rate ($L.s^{-1}$).

Adsorbed amounts of oxoanions (q_{ads}) and saturation adsorption capacities (Q_{sat}) are given by the following relations:

$$q_{ads}\,(mg) = D\,.C_0.\,A$$

$$Q_{sat}\left(mg.g^{-1}\right) = \frac{D\,.C_0.\,A}{m_{CA}}$$

D, C_0, A and m_{CA} correspond to the flow rate ($mL.min^{-1}$), the concentration at the inlet of the column ($mg.L^{-1}$), the area surface corresponding to the adsorbed amount of MnO_4^- (min) and the activated carbon mass used (g) respectively.

Removal percentage (%E) of manganese oxoanions (MnO_4^-) on activated carbon is given by the relation:

$$\%E = \frac{A}{t_{sat}} x100$$

Where t_{sat} is the saturation time (min).

2.5. Adsorption Mechanism of MnO_4^-

Kinetic study of adsorption processes provides information on the adsorption mechanism and the mode of transfer of solutes from the liquid phase to the solid phase. In order to evaluate these parameters, the pseudo-first-order kinetic models developed by Lagergren [34], the pseudo-second order developed by Blanchard and linearized by Ho [36,37] and the Weber and Morris model [38] were applied to experimental data of MnO_4^- breakthrough curves.

The rate law of a pseudo-first-order reaction is expressed by the following relation [33]:

$$\frac{dQ_t}{dt} = k(Q_e - Q_t)$$

After integration between t = 0 and t, and at $Q_t = 0$ and Q_t. We then obtain the following linear form:

$$\log(Q_e - Q_t) = \log Q_e - \frac{k_1}{2,3}.t$$

Q_t and Q_e correspond to the adsorption capacities at time t and equilibrium ($mg.g^{-1}$) respectively, and k_1 the adsorption rate constant of the pseudo-first order kinetic model (min^{-1}).

The pseudo-second order model is expressed by the following relation [36]:

$$\frac{dQ_t}{dt} = k_2 (Q_e - Q_t)^2$$

After integration between t = 0 and t, then when $Q_t = 0$ and Q_t, we obtain the following linear form [37]:

$$\frac{t}{Q_t} = \frac{1}{k_2 . Q_e^2} + \frac{1}{Q_e} . t$$

Q_t and Q_e correspond to the adsorption capacities at time t and equilibrium ($mg.g^{-1}$) respectively, and k_2 the adsorption rate constant of the pseudo-first order kinetic model ($g.mg^{-1}.min^{-1}$).

According to Webber and Morris [37], the kinetic expression of intraparticle diffusion is showed by:

$$Q_t = k.t^{1/2} + C_d$$

Where k_d is the intraparticle diffusion rate constant ($mg.g^{-1}.min^{1/2}$) and C_d, intercept of the curve. This gives an indication of the thickness of the boundary layer and/or adhesion to the surface.

3. Results et Discussion

3.1. Adsorbent Characteristics

In order to evaluate the textural and chemical characteristics of the prepared activated carbon, textural analysis by nitrogen (N_2) physisorption was performed. Determination of pH at point of zero charge (pH_{PZC}) and the quantification of surface function groups were also performed.

The N_2 physisorption isotherm obtained on the activated carbon studied is shown in Figure 2. The form of the isotherm obtained describes a type I isotherm according to the IUPAC classification [39]. This isotherm is characteristic of microporous materials with a hysteresis loop of type H4, which indicates the presence of pores in the form of a slit. The specific surface area BET (S_{BET}) and the microporous volume obtained after exploitation of the isotherm of N_2 physisorption are 116.2 $m^2.g^{-1}$ and 0.046 $cm^3.g^{-1}$ respectively (Table 1).

Table 1. Structural and chemical characteristics obtained on the studied activated carbon.

S_{BET} ($m^2.g^{-1}$)	$V_{micro.}$ ($cm^3.g^{-1}$)	$V_{meso.}$ ($cm^3.g^{-1}$)	$V_{total\ pore}$ ($cm^3.g^{-1}$)	Average pore size (nm)	pH_{PZC}	Basic fonctions ($mmol.g^{-1}$)	Acidic fonctions ($mmol.g^{-1}$)			
							Total	Carboxyl	Lactone	Phenol
116.2	0.046	0.002	0.049	1.698	6.7	0.6	3.2	0.2	0.63	2.4

The results in Table 1 also confirm the absence of mesopores. Indeed, the mesoporous volume (0.002 $cm^3.g^{-1}$) is insignificant compared to microporous volume (0.046 $cm^3.g^{-1}$) obtained on the AC studied.

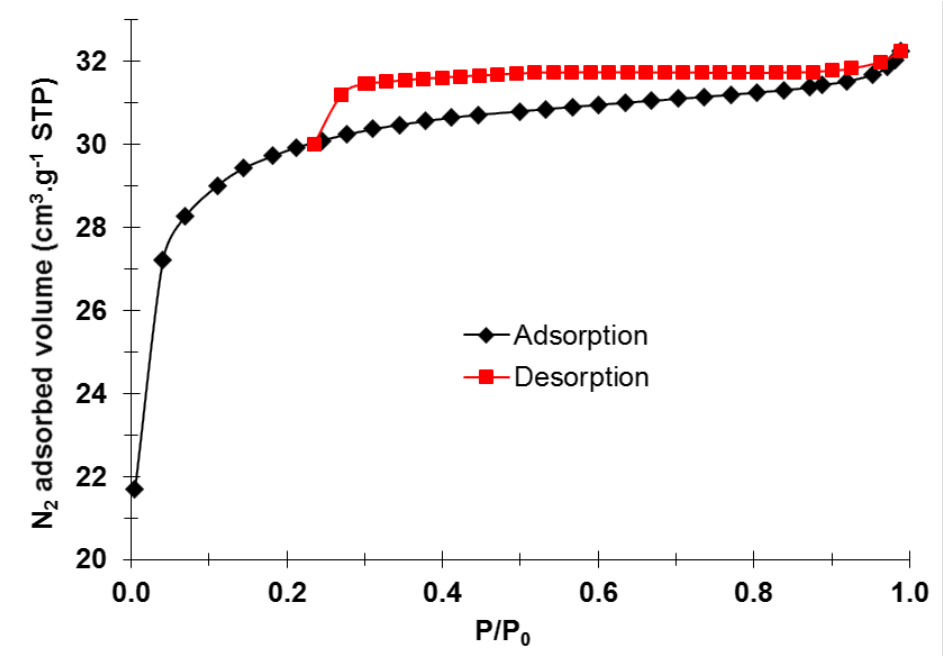

Figure 2. Isotherm of N_2 adsorption/desorption obtained at 77 K on the studied activated carbon

According to Figure 3, the pH at point of zero charge (pH_{PZC}) of AC studied is equal to 6.7. This result indicates that the surface of activated carbon is positively charged when the pH of the solution (pH_{sol}) is less than 6.7 and is negatively charged when the pH is above 6.7. Thus, interactions between the surface of activated carbon and manganese oxoanions (MnO_4^-) will be more favorable or important at $pH_{sol} < pH_{PZC}$.

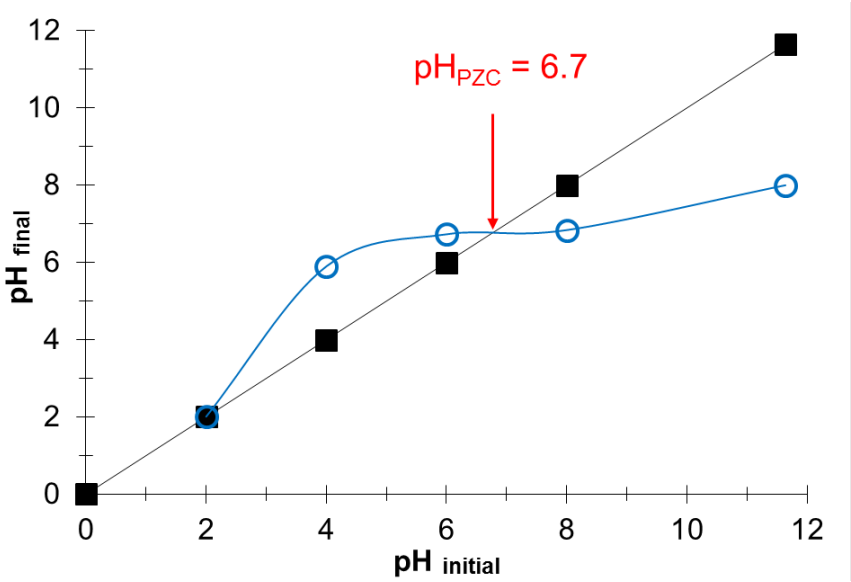

Figure 3. Determination of pH at the point of zero charge (pH_{PZC}) on the activated carbon studied

Results of the determination of concentrations of surface functions of the activated carbon studied are summarized in Table 1. These results show that the amounts of acid groups (3.2 mmol.g^{-1}) are greater than those of basic groups (0.3 mmol.g^{-1}). They indicate also that phenol groups are predominant among acid oxygen functions (carboxyl) followed by lactone groups on the surface of prepared activated carbon.

3.2. Dynamic Adsorption on Fixed-bed Column of MnO_4^-

The objective of this study was to evaluate the influence of operating parameters on the adsorption capacities of granular activated carbon (GAC) that constitute the bed under dynamic conditions. Thus, studies on the effect of particle size (x), initial solution concentration (C_0) of MnO_4^-, flow rate (D) and media pH were performed. This in order to find the optimal operating conditions for a better removal of manganese oxoanions on the prepared activated carbon.

3.2.1. Effect of Particle Size

Since adsorption is a surface phenomenon and the efficiency of its process should be proportional to the available specific surface area of the adsorbent, particle size is therefore an important factor in adsorption processes. Results of the study of the influence of particle size on the adsorption of MnO_4^- ions are grouped in Table 2.

Results show that the more the particle size decreases, the more the adsorbed amounts of MnO_4^- (q_{ads}) and bed saturation capacities (Q_{sat}) increase. Indeed, Q_{sat} of GAC bed of particle sizes 0.04 <x< 0.1 mm (5.9 mg.g^{-1}) is higher than those of particle sizes 0.1 <x< 0.25 mm (3.1 mg.g^{-1}) and 0.25 <x< 0.5 mm (1.3 mg.g^{-1}). This increase in adsorption capacities is related to the fact that beds composed of small particles have larger surface areas and consequently, greater distribution of adsorption sites.

Figure 4 shows the breakthrough curves of MnO_4^- obtained on the GAC with different particle sizes. All breakthrough curves obtained show a multi-step adsorption mode (3 zones) in the form of staircase, with different adsorption kinetics and diffusions according to form of slopes of each adsorption domain.

The first step (0 - 50 min) seems to indicate an adsorption kinetic and a rapid diffusion of the aqueous phase containing MnO_4^- on the surface of the adsorbent and on easily accessible sites. This reveals weak interactions between the structure of the adsorbent and the MnO_4^- ion according to the slopes of the curves of this domain (Figure 4). In this zone (0 - 50 min), the 0.04<x<0.1 mm particle size bed, compared to the other two beds, appears to show slow diffusion and/or stronger adsorbate-adsorbent interactions. Indeed, the slope obtained is more inclined compared to the other two beds of GAC (Figure 4).

The second zone (50 - 150 min) and the third (> 150 min) are zones corresponding respectively to intraparticle and surface adsorption of the oxoanions (MnO_4^-) on hardfull access sites of the prepared GAC. The slopes of these adsorption zones tend toward horizontal, indicating slow adsorption kinetics and diffusion of MnO_4^- at the surface or between the grains of the adsorbent with strong adsorbent-adsorbent interactions greater than those observed in zone 1 (0 - 50 min).

Table 2. Results of the adsorption of MnO_4^- in fixed-bed dynamics obtained on GAC at 298 K at different particle sizes with C_0 = 50 mg.L^{-1}, pH = 6.5 and H = 0.5 cm.

Particle sizes (mm)	t_c (s)	t_{sat} (min)	q_{ads} (mg)	Q_{sat} (mg.g^{-1})	%E
0.25 < x < 0.5		100	0.61	1.39	4.5
0.1 < x < 0.25	45	155	1.52	3.05	6.5
0.04 < x < 0.1		270	3.50	5.90	7.0

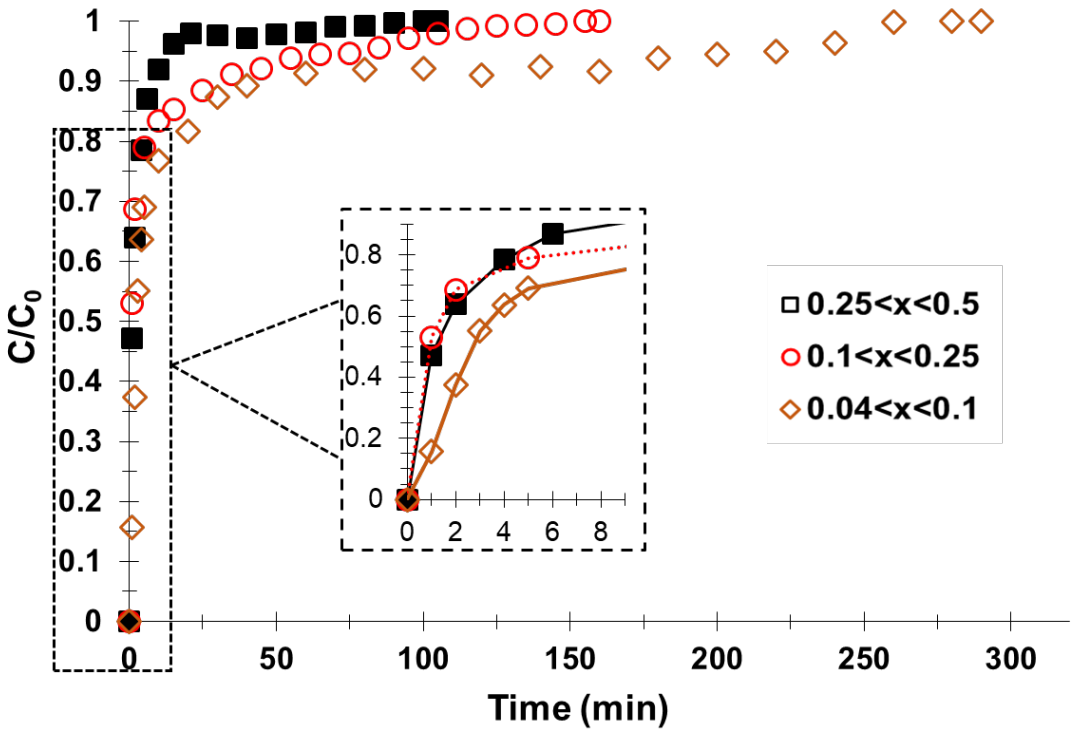

Figure 4. Breakthrough curves of MnO_4^- obtained at 298 K on the beds of the prepared GAC composed of particles of different sizes with H = 0.5 cm, D = 3 $mL.min^{-1}$, C_0 = 50 $mg.L^{-1}$ and pH = 6.5

These breakthrough curves show also a very low affinity of MnO_4^- with the CAG under our operating conditions (Figure 4). On the other hand, the saturation times obtained (Table 2) indicate that the prepared GAC has adsorption sites favorable to interactions of MnO_4^- with the GAC structure. The saturation time of the bed composed of particle size 0.04<x<0.1 mm is 270 min, which is higher compared to those of GAC beds of particle size 0.1<x<0.25 mm and 0.25<x<0.5 mm (155 and 100 min respectively). This is mainly due to the fact that smaller particles have higher flow resistance and a shorter scattering path in the pores, allowing MnO_4^- to easily access the surface of the GAC particle [39].

Finally, we realize that the variation in particle size influences the adsorption capacity of MnO_4^- on GAC in our operating conditions. According to the results obtained, the activated carbon bed of low particle size 0.04<x<0.1 mm is the most likely for the removal of MnO_4^- ions. Indeed, this bed shows a more accessible surface and adsorption sites and consequently, a better affinity between MnO_4^- and the adsorbent structure.

3.2.2. Effect of Initial Concentration (C_0) of MnO_4^- Solution

The adsorbate concentration is also important in fixed-bed adsorption system because it determines the mass transfer in the solid phase. Results obtained from the study of the influence of the initial concentration of MnO_4^- on GAC are presented in Table 3.

Results show that q_{ads} and Q_{sat} decrease when the concentration of the initial solution of MnO_4^- decreases. On the other hand, the percentage of elimination (%E) increases. Indeed, at C_0 = 50 $mg.L^{-1}$, the Q_{sat} value (8.4 $mg.g^{-1}$) is higher than those obtained with solutions at 25 $mg.L^{-1}$ and 10 $mg.L^{-1}$ (6.9 and 6.5 $mg.g^{-1}$ respectively). The percentage of removal (% E) of MnO_4^- from a solution at 50 $mg.L^{-1}$ (17.2%) is lower than that obtained with solutions at 25 and 10 $mg.L^{-1}$ (22.9% and 34.5% respectively).

The decrease in adsorption capacities when the concentration decreases would be due to the effect of the concentration gradient considered to be the driving force of the adsorption process [40]. When this gradient decreases, the mass transfer is less important. Thus, the amount adsorbed on the surface and the adsorption capacity of the bed decrease. This phenomenon can also be attributed to a major occupation of adsorption sites. The more there are MnO_4^- ions in the media and in contact with GAC particles, the more the surface sites will be occupied and consequently a significant capacity of the adsorbed species bed [40]. On the other hand, the increase in the percentage of removal (%E) when C_0 decreases would be due to the ratio of MnO_4^- species / GAC particles, which is in favor of GAC because of low amounts of MnO_4^- present in solution [40].

Table 3. Results of the adsorption of MnO_4^- in fixed-bed dynamics obtained on GAC at 25 °C at different initial concentrations of the solution of MnO_4^- (C_0) with D = 3 $mL.min^{-1}$; pH = 6.5; H = 1 cm and bed particle size 0.04<x<0.01

C_0 ($mg.L^{-1}$)	t_c (s)	t_{sat} (min)	q_{ads} (mg)	Q_{sat} ($mg.g^{-1}$)	%E
10		1180	9.90	6.5	34.5
25	90	600	10.31	6.9	22.9
50		490	12.56	8.4	17.2

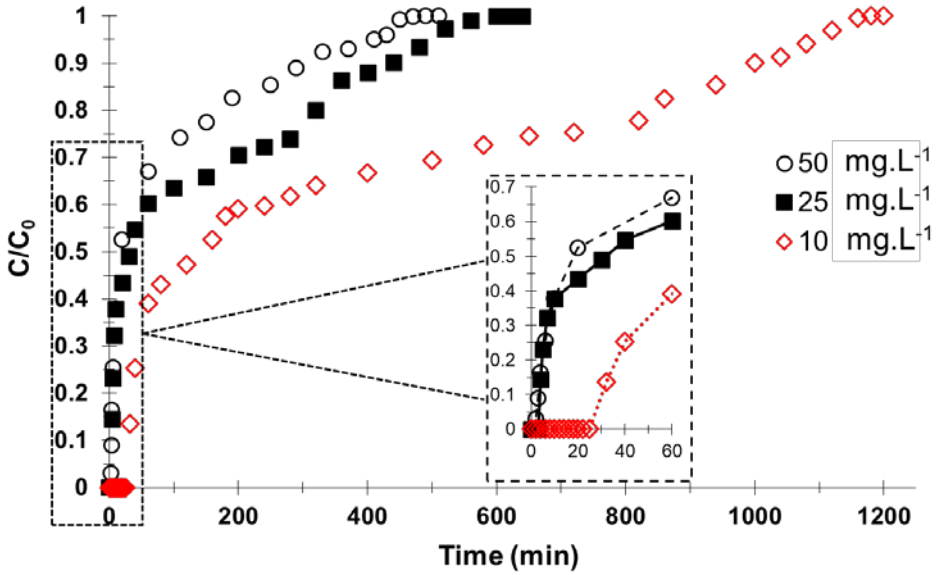

Figure 5. Breakthrough curves of MnO_4^- obtained on GAC prepared at 298 K at different initial concentrations of the solution of MnO_4^- (C_0) with D = 3 mL.min^{-1}; pH = 6.5; H = 1 cm and bed particle size 0.04<x<0.01

However, the breakthrough curves of MnO_4^- obtained (Figure 5) show that the bed is more effective when the concentration of the initial solution is 10 mg.L^{-1}. According to these curves, breakthrough and saturation times increase when the concentration decreases as seen in Figure 4 and Table 3.

The breakthrough start and saturation times of the bed at C_0 = 10 mg.L^{-1} (30 and 1180 min respectively) are superior to those obtained with solutions at C_0 = 25 mg.L^{-1} (4 and 600 min respectively) and 50 mg.L^{-1} (2 and 490 min respectively). It appears that at low concentrations, adsorption sites on the surface of the prepared GAC are slowly occupied by MnO_4^-. Contrarily, high concentrations of MnO_4^- rapidly saturate the bed of the adsorbent.

Slopes of breakthrough curves obtained (Figure 5) reflect this slow sites occupation when C_0 = 10 mg.L^{-1} and rapid saturation at C_0 = 50 mg.L^{-1}. Indeed, the more C_0 increases, the more the diffusion processes are fast and / or the adsorbent interactions /MnO_4^- are weak.

The variation in the initial concentration of the manganese oxoanion (MnO_4^-) solution influences the adsorption capacity of the bed. The GAC bed is more effective for a MnO_4^- solution at C_0 = 10 mg.L^{-1} in our operating conditions.

3.2.3. Effect of Flow Rate

The flow rate affects the efficiency of the fixed-bed adsorption system. Indeed, it determines the sufficient contact time between the adsorbate and the adsorbent. That contact time should be responsible of better elimination of pollutants within the column. Results obtained from the study of the influence of flow rate on adsorption capacities of the prepared GAC are grouped in Table 4.

These results show that the percentage of elimination (%E), q_{ads} and Q_{sat} decrease when the flow rate increases. Indeed, the saturation capacity of GAC, for a flow rate of 3 mL.min^{-1} (8.4 mg.g^{-1}) is higher than those obtained with flow rates 6 and 9 mL.min^{-1} (3.8 and 5.6 mg.g^{-1} respectively). This decrease in adsorption capacity when flow rate increases appears to be related to rapid movement of the mass transfer zone when flow rate increases [40].

Figure 6 shows the breakthrough curves of MnO_4^- obtained. As in previous cases, the multi-step adsorption process of MnO_4^- on the prepared GAC is always observable regardless of the flow rate applied. This process is more marked on the breakthrough curve of MnO_4^- obtained with a flow rate of 3 mL.min^{-1}. For high flow rates, the diffusion of the aqueous phase seems to be very low, thus limiting the interactions between the adsorption sites and MnO_4^-, as shown on the slopes of breakthrough curves obtained with flow rates 6 and 9 mL.min^{-1} (Figure 6).

From breakthrough curves obtained, bed saturation occurs earlier with flow rates 9 and 6 mL.min^{-1} (140 min and 240 min respectively). This indicates that the mass transfer zone flows through the GAC bed faster when the flow rate increases. This leads to a reduction of breakthrough start and saturation times of bed. The amounts of MnO_4^- ions adsorbed are also reduced (Table 4). In addition, an effect of contact time is also observed. The more important the contact time, better are the amounts adsorbed and also the saturation capacity of the bed and the percentage of elimination (Table 4).

Table 4. Results of adsorption of MnO_4^- in fixed-bed dynamics obtained on prepared GAC at 298 K at different flow rates (D) with C_0 = 50 mg.L^{-1}; pH = 6.5; H = 1 cm and bed particle size 0.04<x<0.01

D (mL.min^{-1})	t_c (s)	t_{sat} (min)	q_{ads} (mg)	Q_{sat} (mg.g^{-1})	%E
3	90	490	12.6	8.4	17.2
6	45	240	8.4	5.6	11.6
9	30	150	5.7	3.8	9.0

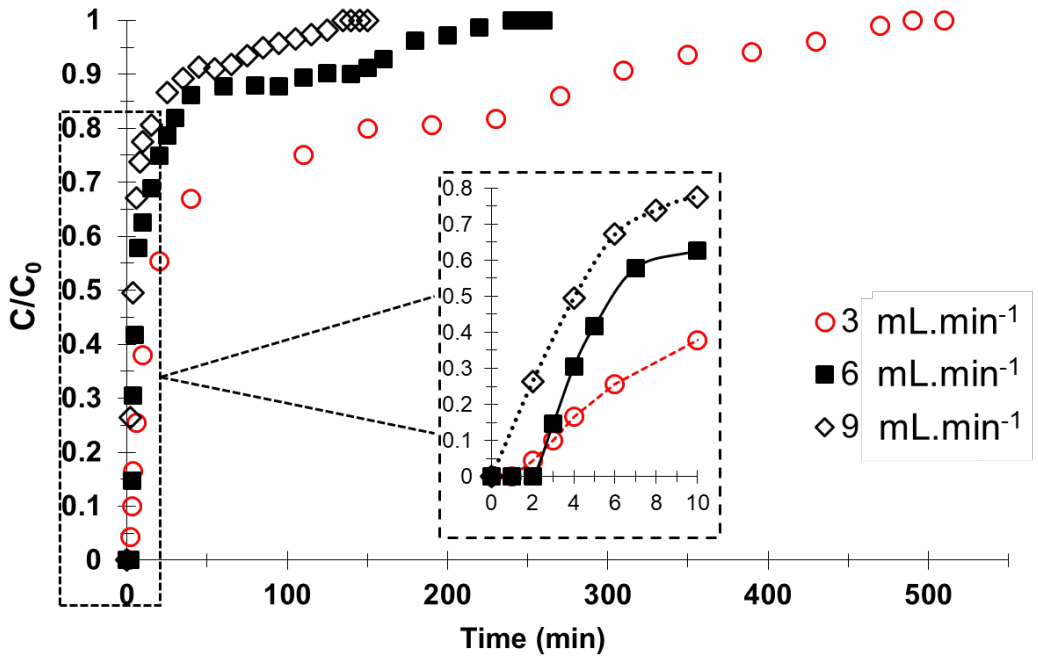

Figure 6. Breakthrough curves of MnO_4^- obtained on prepared GAC at 298 K at different flow rates (D) with C_0 = 50 mg.L^{-1}; pH = 6.5; H = 1 cm and bed particle size 0.04<x<0.01

Thus, the variation in flow rate influences the adsorption capacity of the prepared GAC bed. Based on results obtained, 3 mL.min^{-1} is the most suitable flow rate for better interactions between GAC and the MnO_4^- ions in our operating conditions.

3.2.4. Effect of pH

pH is an important factor in all adsorption processes. This parameter influences both the overall charge of the adsorbent and the structure of the adsorbate, as well as the adsorption mechanism. Results of the study of the effect of pH on MnO_4^- adsorption capacities of the prepared GAC are grouped in Table 5.

Results show that when the pH decreases, the percentage of removal (%E), adsorbed amounts (q_{ads}) and adsorption capacities at saturation of GAC bed (Q_{sat}) increase. Indeed, Q_{sat} at pH 3.5 (27 mg.g^{-1}) is higher than those obtained at pH 4.5 and 6.5 (20.3 and 8.4 mg.g^{-1} respectively). This indicates that the oxoanion MnO_4^- in acidic media, undergoes a strong attraction of surface functions characterized previously, which are affected by the following protonation effect [41]:

$$(\text{Carboxyl})\text{-COOH}+H^+ = \text{-COOH}_2^+;$$

$$(\text{Phenol})\text{-C-OH}+H^+ = \text{-C-OH}_2^+;$$

$$(\text{Lactone})\text{-C=O}+H^+ = \text{-C=OH}^+ \text{ etc.}$$

This protonation of the adsorbate surface enhances the attraction between MnO_4^- and the prepared GAC surface and leads to significant adsorbed amounts and adsorption capacity [42]. This hypothesis suggests physical interactions (physisorption) between MnO_4^- and the prepared GAG. Also in acidic media, the central ion Mn^{VII} of the anion MnO_4^- can be reduced to Mn^{2+} in the presence of electro-donor groups. In other terms, surface functions possessing the oxygen atom, nitrogen and others depend on the reaction:

$$MnO_4^- + 5e^- + 8H^+ = Mn^{2+} + 4H_2O$$

The resulting Mn^{2+} ions would then react with the acid functions that are ionized in an aqueous media (-COOH = -COO-, C-OH = C-O-, etc.) [43,44]. In this case, the MnO_4^- adsorption on the prepared GAC would be a chemisorption with modification of the structure of the adsorbate (Mn^{VII} = > Mn^{2+}) when the media is highly acidified.

Figure 7 shows the breakthrough curves of MnO_4^- obtained on the prepared GAC. These curves also show, as in previous studies, a multi-steps adsorption profile. The diffusion processes and/or interactions between MnO_4^- and activated carbon surface are comparable, regarding breakthrough curves at pH 3.5 and 4.5, especially after a breakthrough time of more than 100 minutes. The diffusion between the grains or on the adsorbent surface of the aqueous phase containing MnO_4^- seems to be slow with strong adsorbent/adsorbate interactions depending on the slopes obtained in these regions.

Table 5. Results of adsorption of MnO_4^- in fixed-bed dynamics obtained on GAC prepared at 298 K at different pH of the solution of MnO_4^- with C_0 = 50 mg.L^{-1}; D = 3 mL.min^{-1}; H = 1 cm and bed particle size 0.04<x<0.01

pH	t_c (s)	t_{sat} (min)	q_{ads} (mg)	Q_{sat} (mg.g^{-1})	%E
3.5		960	40.5	27.0	28.1
4.5	90	760	30.4	20.3	20.3
6.5		490	12.6	8.4	17.2

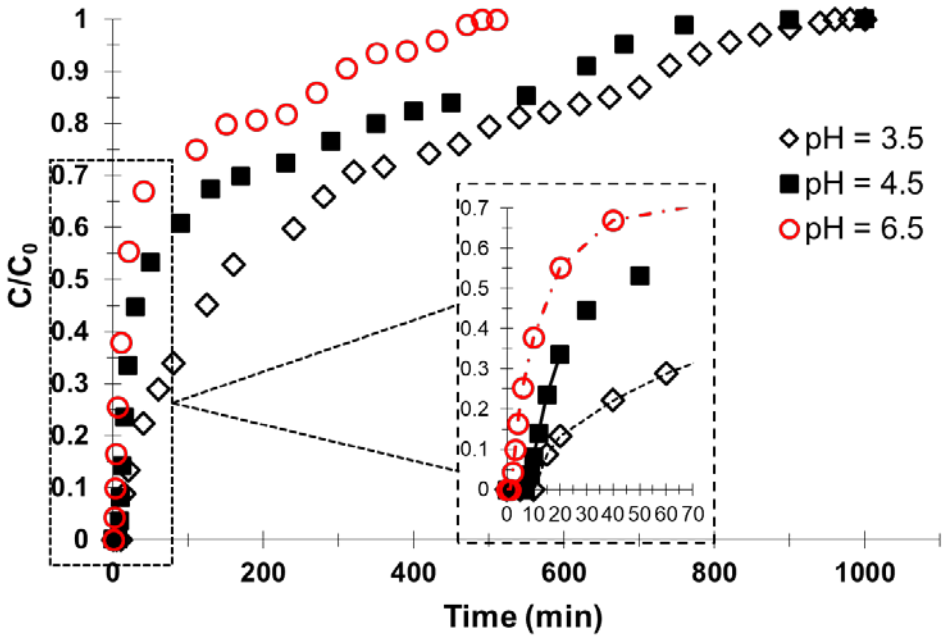

Figure 7. Breakthough curves of MnO_4^- obtained on prepared GAC at 298 K at different pH of initial solution of MnO_4^- with C_0 = 50 mg.L^{-1}; D = 3 mL.min^{-1}; H = 1 cm and bed particle size 0.04<x<0.01

The hypothesis of a MnO_4^- chemisorption seems to be verified in an acidic media. In addition, slower MnO_4^- adsorptions at pH 3.5 and 4.5 are observable compared to that at pH 6.5 (Figure 7), marked by longer bed saturation times (Table 5). This could be explained by the increase in electrostatic attraction forces due to positive charged surface functions, thus reflecting an increase in interactions between GAC and MnO_4^- particles.

Based on the results, it appears that the prepared GAC bed has more affinity with MnO_4^- ions when the media is acidic. The saturation capacities of prepared GAC at pH 3.5 are equal to 27 mg.g^{-1}, greater than 8.4 and 20.2 mg.g^{-1} corresponding respectively to saturation capacities of GAC with MnO_4^- solutions of pH 6.5 and 4.5.

3.3. Adsorption Kinetics of MnO_4^-

The objective of this part is to perform kinetic modeling of MnO_4^- adsorption on the prepared GAC in fixed-bed dynamics in order to identify the kinetics that control the adsorption mechanism of MnO_4^- ions on GAC in our operating conditions. Pseudo-first and pseudo-second order kinetics and intraparticle diffusion models were applied to experimental data from the various studies previously performed.

3.3.1. Pseudo-first and Pseudo-second Order Kinetic Models

Figure 8 shows the linearization curves of pseudo-first-order (Figure 8a) and pseudo-second-order kinetic models (Figure 8b) applied to experimental data from the above study concerning the influence of pH on the MnO_4^- adsorption capacities in fixed-bed dynamics. From these curves, it seems that the pseudo-first-order kinetics model shows better linearization of experimental points compared to the pseudo-second-order kinetic model for adsorption times up to 300 minutes.

Table 6 summarizes the studied operating parameters, the experimental values of equilibrium adsorption capacities ($Q_{e,\,exp.}$) and the characteristic parameters ($Q_{e,cal.}$, rate constants (k) and linear regression coefficient (R^2)) of pseudo-first and pseudo-second order kinetic models related to the different studies carried out.

Results obtained indicate that the pseudo-first-order kinetic model is the model that best describes the MnO_4^- ions adsorption in fixed-bed dynamics on the prepared GAG. Indeed, contrary to the results of the pseudo-second-order model (Table 6), the calculated equilibrium adsorption capacities ($Q_{e\ cal.}$) are very close to those obtained experimentally ($Q_{e,\ exp.}$). Moreover, the correlation coefficients (R^2) obtained for the pseudo-first order is also very close to the unit for all results (R^2 = 0.999). These results are different from those obtained by Al-Aoh [45] on the kinetic study for potassium permanganate adsorption by Neem leaves powder where the adsorption of MnO_4^- ions in static mode on Neem leaves powder follows a pseudo-second-order kinetic.

In addition, results in Table 6 show that the rate constant k_1 increases when D, C_0 and particle size increase. This indicates that when D, C_0 and particle size increase, we have rapid bed saturation and therefore reduced bed efficiency. On the other hand, k_1 decreases when the pH of the initial solution decreases (Table 6). This means that we have a slower saturation of bed due to the increase of adsorption sites by protonation of surface functions when the solution is acidic and therefore, an increase in the efficiency of bed. These results are in agreement with those obtained during the study of the influence of these parameters on the MnO_4^- adsorption capacities of prepared GAC.

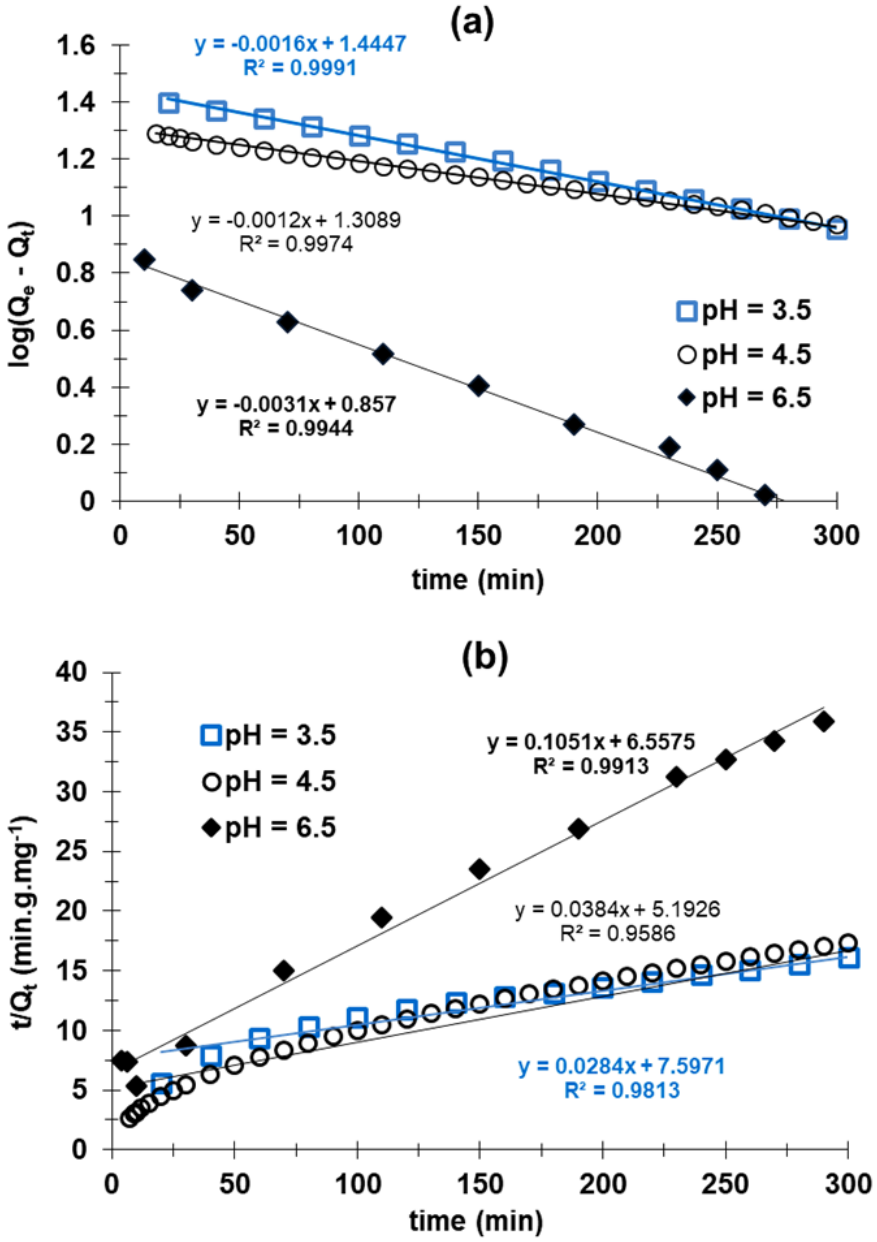

Figure 8. Models of pseudo-first-order (a) and pseudo-second-order (b) kinetics applied to experimental data from the fixed-bed dynamic adsorption study of MnO_4^- on prepared GAC at different pH of the initial MnO_4^- solution

Table 6. Experimental conditions and experimental Qe values and parameter values of pseudo-first and pseudo-second-order kinetic models of fixed-bed dynamic adsorption of MnO_4^- on the prepared GAC

	Experimental		Parameters of kinetic models					
			Pseudo-first-order			Pseudo-second-order		
	Conditions	$Q_{e,exp.}$ ($mg.g^{-1}$)	$Q_{e,cal.}$ ($mg.g^{-1}$)	k_1 (min^{-1})	R^2	$Q_{e,cal.}$ ($mg.g^{-1}$)	k_2 ($g.mg^{-1}.min^{-1}$)	R^2
pH	3.5	27.01	27.99	0.00368	0.999	0.13	2032	0.981
	4.5	20.28	20.81	0.00253	0.997	0.12	4414	0.959
	6.5	8.36	8.44	0.00690	0.994	0.11	373	0.991
C_0 ($mg.L^{-1}$)	10	6.48	6.98	0.00184	0.991	0.03	8921	0.996
	25	6.89	6.60	0.00115	0.997	0.05	2834	0.924
	50	8.36	8.44	0.00690	0.995	0.11	373	0.991
D ($mL.min^{-1}$)	3	8.36	8.44	0.00690	0.995	0.11	373	0.991
	6	5.58	4.97	0.01173	0.991	0.16	223	0.953
	9	3.79	3.35	0.02300	0.988	0.39	25	0.988
particle size (mm)	0.1<x<0.04	5.90	5.06	0.00851	0.992	0.14	292	0.954
	0.1<x<0.25	3.05	2.36	0.01403	0.995	0.17	218	0.982
	0.25<x<0.5	1.39	1.45	0.01449	0.994	0.21	27	0.994

3.3.2. Intraparticle Kinetic Model

Figure 9 shows the kinetic model of Weber and Morris (intraparticle diffusion model) applied to the experimental data of the study concerning the influence of pH on the adsorption capacities of the prepared GAC in fixed-bed dynamics adsorption. The curves obtained show multilinear regions (2 regions) for the adsorbent studied. This result confirms the hypothesis that fixed-bed adsorption of MnO_4^- ions on the prepared GAC follows a multi-step adsorption process. Al-Aoh [45] also obtained similar results in his work.

The values of the constants C_d and intraparticle diffusion rates k_d, as well as the linear regression coefficients R^2 of the different zones, obtained after applying the intraparticle diffusion model on the experimental data of the different studies, are presented in Table 7. Results show that linear regression lines have good correlation coefficients but do not pass through the origin ($C_d \neq 0$), which means that intraparticle diffusion is involved in the mechanism of MnO_4^- adsorption on the prepared GAG, but is not the limiting step and the only process governing the adsorption of manganese oxoanions on GAC in dynamic adsorption on fixed-bed column.

The intercept curve C_d of different linear domains (Table 7) represents the thickness of the boundary layer (C_d). The greater the C_d value, the greater the contribution to surface adhesion in the speed limit step [37]. C_{d2} values are particularly high. This confirms the fact that intraparticle diffusion is not the limiting step, and rather that surface adsorption plays a predominant role in the adsorption of MnO_4^- ions on the prepared GAC in our operating conditions.

Also, in an acidic medium (pH = 3.5) the surface adhesion is very high, especially in zone 2 (C_{d2} = 9.151). This result confirms the protonation of surface functions on the prepared GAC in acidic media thus creating new adsorption sites and/or strong interactions between MnO_4^- / GAC on the surface. The hypothesis in acidic media of a chemisorption of MnO_4^- ions still seems to be valid.

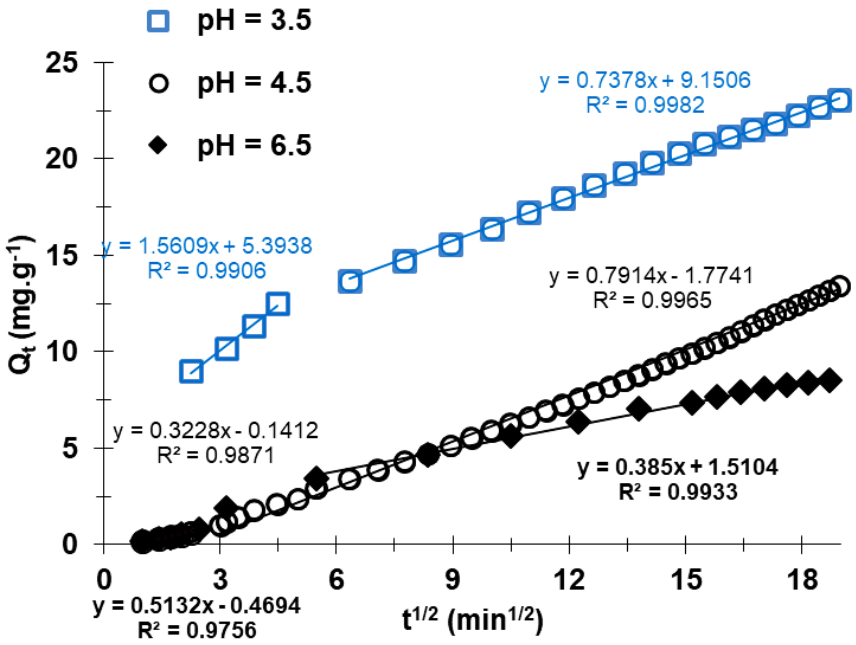

Figure 9. Intraparticle kinetic model applied to experimental data from the study of fixed-bed dynamic adsorption of MnO_4^- on the prepared GAC at different pH of the initial MnO_4^- solution

Table 7. Experimental conditions and parameter values of the intraparticle kinetic model of fixed-bed dynamic adsorption of MnO_4^- on the prepared GAC

		Region 1			Region 2		
		$k_{dif.1}$ (mg.min$^{-1/2}$.g^{-1})	C_{d1}	R^2	$k_{dif.2}$ (mg.min$^{-1/2}$.g^{-1})	C_{d2}	R^2
pH	3.5	1.561	5.394	0.991	0.738	9.151	0.998
	4.5	0.328	0.141	0.987	0.791	1.774	0.997
	6.5	0.513	0.469	0.976	0.385	1.510	0.993
C_0 (mg.L^{-1})	10	0.883	2.561	0.996	0.123	1.676	0.997
	25	1.677	1.251	0.994	0.109	4.592	0.978
	50	2.032	3.103	0.994	0.095	7.689	0.984
D (mL.min^{-1})	3	2.356	3.037	0.999	0.104	7.829	0.994
	6	0.576	1.325	1.000	0.321	1.672	0.991
	9	0.316	2.172	1.000	0.196	2.623	0.991
Particle size (mm)	0.1<x<0.04	0.756	1.602	0.994	0.268	2.465	0.996
	0.1<x<0.25	0.273	1.250	0.997	0.138	1.357	0.996
	0.25<x<0.5	0.033	0.811	0.994	0.100	0.624	0.995

4. Conclusion

Objective of these experiments was to study the influence of operating parameters such as particle size, concentration of the initial solution (C_0) of manganese oxoanion (MnO_4^-), flow rate (D) and pH of the media on the adsorption capacities of granular activated carbon (GAC), prepared from palm nuts shells, in dynamic adsorption on fixed-bed column. Also, the adsorption kinetics of MnO_4^- on prepared GAC were studied.

The prepared activated carbon has been characterized texturally and chemically. Characterization by physisorption of nitrogen (N_2) reveals a mainly microporous structure with a specific surface area (S_{BET}) of 116.2 $m^2.g^{-1}$ and a microporous volume equal to 0.046 $cm^{-3}.g^{-1}$. The determination of surface functions indicates that the concentration of acid groups (3.2 $mmol.g^{-1}$) is greater than that of basic groups (0.3 $mmol.g^{-1}$). The pH at the point of zero charge (pH_{PZC}) of prepared activated carbon was evaluated at 6.7.

Study of the influence of operating parameters on the saturation adsorption capacities (Q_{sat}) of prepared activated carbon in fixed-bed dynamics shows an increase of adsorption capacities when the particle size decreases, the flow rate (D) decreases, the concentration of MnO_4^- ions (C_0) increases and when the pH decreases. Best Q_{sat} of manganese oxoanion on GAC were obtained when, following the study, the MnO_4^- adsorption was carried out with a particle size $0.04 < x < 0.1$ (5.90 $mg.g^{-1}$); a flow rate of 3 $mL.min^{-1}$ (8.36 $mg.g^{-1}$) and at pH 3.5 (27.01 $mg.g^{-1}$). Also, the bed of prepared GAC appears more effective at $C_0 = 10\ mg.L^{-1}$.

Kinetic models of the different studies carried out show that the pseudo-first-order kinetic model best describes the adsorption of MnO_4^- ions on the GAC. The results of the intraparticle diffusion model indicate that the adsorption of MnO_4^- follows a multi-step process and that the intraparticle diffusion is not the limiting step. In addition, the surface adsorption plays a predominant role in the adsorption mechanism of MnO_4^- ions on activated carbon studied in fixed-bed column dynamics.

References

[1] Eric FOTO, Oscar ALLAHDIN, Olga BITEMAN, Nicole POUMAYE, and Seraphin PINIKO, "Assessment of Water Contamination by Metallic Trace Elements at Mining Sites: The Case of the Ouham River in the Central African Republic." American Journal of Environmental Protection, vol. 10, no. 2 (2022): 47-56.

[2] Messi Me Ndong, A.N., Bouraima, A., Bissielou, C., Anguile, J.J. and Makani, T. (2021) Chemical Composition Assessment by Wavelength Dispersive X-Ray Fluorescence of Agricultural Soils in the Mining Town of Moanda, Gabon. Journal of Agricultural Chemistry and Environment, 10, 345-358.

[3] République Gabonaise, Direction Générale du Trésor, Ministère de l'Economie, des Finances et de la Relance (2021).

[4] Koumba, C. (2014) La gestion et l'exploitation des ressources naturelles au Gabon: vers une réorganisation spatiale des activités productives. Les Cahiers d'Outre-Mer, p 256.

[5] Jinbei Yang, Meiqiong Yu, Wentao Chen, Adsorption of hexavalent chromium from aqueous solution by activated carbon prepared from longan seed: Kinetics, equilibrium and thermodynamics, Journal of Industrial and Engineering Chemistry, Volume 21(2015), Pages 414-422.

[6] Oladoja N A, Unouabonah E L. Progress And Prospect In The Management Of Oxyanions Polluted Aqua Systems. Environmental Contamination Remediation and Management (2021).

[7] Mbaye G. (2009). Synthèse et étude des charbons actifs pour le traitement des eaux usées d'une tannerie, Mémoire de Master, Institut Internationale d'Energie de l'Eau et de l'Environnement de Ouagadougou.

[8] Weidner E, Ciesielczyk F. Removal of hazardous oxyanions from the environment using metal-oxide-based. Materials. 2019. 12(6): p. 927.

[9] Water. Edition of the drinking water standards and health advisories. 2012.

[10] Anyiam Ngozi Donald, Pene Barikuma Raphael, Oluwole James Olumide, and Okoro Felicitas Amarachukwu, "Environmental Heavy Metal Pollution: Physicochemical Remediation Strategies to the Rescue." Journal of Environment Pollution and Human Health, vol. 10, no. 2 (2022).

[11] Athéba, G.P., N'guadi, B.A., Dongui, B.K., Kra, D.O., Gbassi, K.G. and Trokourey, A. (2015) Adsorption du Butyllparabène sur du Charbon Activé à base des Coques de Coco Provenant de Cote d'Ivoire. International Journal of Innovation and Scientific Research, 13, 530-541.

[12] Fu F, Wang Q. Removal of heavy metal ions from wastewaters: a review. Journal of environmental management. 2011 Mar 1; 92(3): 407-18.

[13] Abdullah N, Yusof N, Lau WJ, Jaafar J, Ismail AF. Recent trends of heavy metal removal from water/wastewater by membrane technologies. Journal of Industrial and Engineering Chemistry. 2019 Aug 25; 76: 17-38.

[14] Barakat MA. New trends in removing heavy metals from industrial wastewater. Arabian journal of chemistry. 2011 Oct 1; 4(4): 361-77.

[15] Jin W, Du H, Zheng S, Zhang Y. Electrochemical processes for the environmental remediation of toxic Cr (VI): A review. Electrochimica Acta. 2016 Feb 10; 191: 1044-55.

[16] Rathnayake SI, Martens WN, Xi Y, Frost RL, Ayoko GA. Remediation of Cr (VI) by inorganic-organic clay. Journal of colloid and interface science. 2017 Mar 15; 490: 163-73.

[17] Ahmed SF, Mofijur M, Nuzhat S, Chowdhury AT, Rafa N, Uddin MA, Inayat A, Mahlia TM, Ong HC, Chia WY, Show PL. Recent developments in physical, biological, chemical, and hybrid treatment techniques for removing emerging contaminants from wastewater. Journal of hazardous materials. 2021 Aug 15; 416: 125912.

[18] Barakat MA. New trends in removing heavy metals from industrial wastewater. Arabian journal of chemistry. 2011 Oct 1; 4(4): 361-77.

[19] Vareda JP, Valente AJ, Durães L. Assessment of heavy metal pollution from anthropogenic activities and remediation strategies: A review. Journal of environmental management. 2019 Sep 15; 246: 101-18.

[20] Giraudet S. Performances et sécurité des procédés de traitement des composés organiques volatils par adsorption sur charbon actif. Thèse, Université de Nantes, (2007).

[21] Ezeugo J N O, Anadebe C V. Removal of potassium permanganate from aqueous solution by adsorption onto activated carbon prepared from animal bone and corn cob. Journal of Engineering. (2018), (1), 29-36.

[22] Hatem A., Al-Aoh. Equilibrium, thermodynamic and kinetic study for potassium permanganate adsorption by Neem leaves powder. Desalination and water treatment 170 (2019) 101-110.

[23] Bani-Atta S. Potassium permanganate dye removal from synthetic wastewater using a novel, low-cost adsorbent, modified from the powder of Foeniculum vulgare seeds. Scientific Reports, 2022, 12(1), 4547.

[24] Aprilliani F et al. A Kinetic studies of potassium permanganate adsorption by activated carbon and its ability as ethylene oxydation material. Earth and Environnemental science, 141 (2018), 012003.

[25] Aljohani M., Al-Aoh H A. Adsorptive removal of permanganate anions from synthetic wastewater using copper sulfide nanoparticules. Materials Research Express, (2021), 8(3), 035012.

[26] Amola, L.A., Kamgaing, T., Tchuifon, D.R.T., Atemkeng, C.D. and Anagho, S.G. (2020) Activated Carbons Based on Shea Nut Shells (Vitellaria paradoxa): Optimization of Preparation by Chemical Means Using Response Surface Methodology and

Physicochemical Characterization. Journal of Materials Science and Chemical Engineering, 8, 53-72.

[27] T. Belin, C. Mve Mfoumou, S. Mignard, Y. Pouilloux, Study of physisorbed carbon dioxide on zeolites modified by addition of oxides or acetate impregnation, Microporous and Mesoporous Materials, 182 (2013) 109-116.

[28] S. Brunauer, P.H. Emmett, E.J. Teller, J. Am. Chem. Soc. 60 (1938) 309.

[29] B.C. Lippens, J.H. De Boer, J. Catal. 4 (1965) 319.

[30] J.H. De Boer, B.C. Lippens, B.G. Lisen, B.C.P. Broekhoff, A. Van Den Heuvel, T.J. Osinga, J. Colloid Interface Sci. 21 (1966) 405.

[31] J. Lynch, F. Raatz, P. Dufresne, Zeolites 7 (1987) 333.

[32] Boehm, H.P. (1966) Chemical Identification of Surface Groups. Advances in Catalysis, 16, 179.

[33] Maazou, S.D.B., Hima, H.I. and Mousbahou, M. (2017) Elimination du chrome par du charbon actif élaboré et caractérisé à partir de la coque du noyau de Balanites aegyptiaca. International Journal of Biological and Chemical Sciences, 11, 3050-3065.

[34] Goertzen, S.L., et al., Standardization of the Boehm titration. Part I. CO2 expulsion and endpoint determination. 2010. 48(4): p. 1252-1261.

[35] Charly Mve Mfoumou, Pradel Tonda-Mikiela, Francis Ngoye, Thomas Belin, and Samuel Mignard, "Dynamic Adsorption and Desorption of CO2 from Binary Mixtures of CH4 and C3H8 on X Type Zeolites." American Journal of Environmental Protection, vol. 10, no. 2 (2022): 83-90.

[36] Lagergren S., Zur theorie der sogenannten adsorption gel oster stoffe, K sven. Vetenskapsak. Handl. 24, 1-39, 1898.

[37] Blanchard G., Maunaye M., Martin G. Removal of heavy metals from waters by means of natural zeolites. Water Res. 18, 1501-1507, 1984.

[38] HO Y.S., G. MCKAY (1999). Pseudo-second-order model for sorption processes. Proc. Biochem., 34, 451-465.

[39] Weber J. Jr. Adsorption in physicochemical process for water quality control, Ed. By Metcalf R L. et Pitts J N, Weley interscience, N Y, Chap. 5, 199-259, 1972.

[40] IUPAC, Pure Appl. Chem. 57 (4) (1985) 603.

[41] Malkoc, E. and Y.J.J.o.H.M. Nuhoglu, Removal of Ni (II) ions from aqueous solutions using waste of tea factory: Adsorption on a fixed-bed column. 2006. 135(1-3): p. 328-336.

[42] Tan, I., A. Ahmad, and B.J.B.t. Hameed, Fixed-bed adsorption performance of oil palm shell-based activated carbon for removal of 2, 4, 6-trichlorophenol. 2009. 100(3): p. 1494-1496.

[43] Niyaz Mohammad Mahmoodi, Bagher Hayati, Mokhtar Arami, Christopher Lan, Adsorption of textile dyes on pine cone from colored wastewater: kinetic, equilibrium and thermodynamic studies. Powder Technology. 2011. 268(1-3): p. 117-125.

[44] Ji Hae Seo, Namgyu Kim, Munsik Park, Sunkyung Lee, Seungjae Yeon, Donghee Park, Evaluation of metal removal performance of rod-type biosorbent prepared from sewage-sludge, Environmental Engineering Research, 2020. 25(5): p. 700-706.

[45] H.A. Al-Aoh, Desalination and Water Treatment 170 (2019) 101-110.